Ability to discern the splitting between longitudinal and transverse plasmon resonances in Au compared to Ag nanoparticles in close-packed planar arrays

Peng Yang, Hervé Portalès, and Marie-Paule Pileni*
Université Pierre et Marie Curie, UMR 7070, LM2N, 4 Place Jussieu, 75005 Paris, France
and Centre National de la Recherche Scientifique, UMR 7070, LM2N, 4 Place Jussieu, 75005 Paris, France
(Received 29 January 2010; revised manuscript received 30 March 2010; published 5 May 2010; corrected 11 May 2010)

The discrete dipole approximation method is used to simulate the optical response of ultrafine Au nanoparticles (NPs) with a diameter of 5 nm assembled in a planar hexagonal array. Similar calculations performed for Ag NPs arrays are also presented for comparison. For both cases, the absorption spectra are calculated for various incidence angles and interparticle distances to reveal the optical anisotropy related to the geometry of the system through the splitting of the surface-plasmon resonance (SPR) into the transverse and longitudinal modes. This effect usually results in the emergence of two SPR bands in the absorption spectrum as observed for Ag NPs arrays when the border-to-border interparticle distance becomes smaller than around one particle radius. Conversely, such a splitting is shown to be undistinguishable for Au NPs arrays whatever the interparticle distance and the incidence angle are. The different behaviors pointed out between Au and Ag NPs arrays are ascribed to the intrinsic dielectric properties of these two metals.

DOI: 10.1103/PhysRevB.81.205405 PACS number(s): 78.67.−n, 71.45.Gm, 07.05.Tp

I. INTRODUCTION

The interest in the optical properties of noble metals has a long history since the early study of the behavior of gold (and other metals) on exposure to light in 1857.[1] Given the recent development of nanoscience and nanotechnology, the noble-metal nanoparticles (NPs) have attracted great interest for their potential applications in a wide variety of domains such as optics,[2–6] chemical sensoring,[6–8] and medical diagnostics,[6,9,10] etc. This is in relation with their special optical feature, which is the so-called surface-plasmon resonance (SPR). It is well established that the SPR spectra of noble-metal NPs depend on their size, shape, and external dielectric environment.[11,12] Controlling some of these parameters enables artificially manipulating the NPs optical properties in order to fit specific applications. In particular, developing new synthesis routes for the production of NPs with controlled sizes remained, until the recent past, a challenging issue in the roadmap of nanotechnology.

In the last few years, several methods have been successfully developed to synthesize NPs with a narrow size distribution, making it possible to use them as building blocks for the production of two-dimensional (2D) or three-dimensional superlattices. These close-packed NP self-assemblies have been already demonstrated to exhibit collective physical properties differing from both those of individual NPs and bulk materials.[13,14] Interestingly, such collective properties can be tailored by tuning the dipolar interactions between NPs through the change in the interparticle spacing in the array.[15,16] In this attempt, various experimental and theoretical studies have focused on the optical characterization of both the individual and collective plasmon resonances in Au NPs assemblies.[17–25] In particular, several groups reported the fabrication and characterization of Au NPs assemblies in solution by using NPs with a diameter ranging from 13 to 16.6 nm and coated with different surfactants.[21–23] The ultraviolet-visible (UV-Vis) extinction spectra of these solutions were found to exhibit two SPR bands interpreted, in decreasing order of energy, as the usual individual SPR of Au NPs and the contribution of Au NPs aggregates, respectively. Similar features were observed from extinction measurements performed on films containing 13 nm Au NPs and polyelectrolyte multilayer structures deposited on silicon wafers[24] for various interparticle and interlayer spacings. Surprisingly, another study of DNA-linked Au NPs aggregates containing oligonucleotide linkers of varying length showed that the UV-Vis extinction spectra of these aggregates only exhibited one single SPR band whose changes in characteristics (energy and bandwidth) were found to inversely depend on the linker length, ranging from 8 to 24 nm. Hence, from these results, which appear to be somewhat confusing, the actual ability to observe both the SPR of individual NPs and the collective plasmon resonance arising from the dipolar interactions between NPs in such an assembly is still greatly debated.

In this paper, the optical properties of ultrafine Au NPs ordered in hexagonal planar arrays are emphasized using the discrete dipole approximation (DDA) method and compared to those of similarly shaped Ag NPs arrays. The optical anisotropy arising from the 2D symmetry of these systems is examined through the dependence of the SPR spectrum on both the incidence and interparticle spacing. Here, it is found that no splitting of the SPR band into the transverse and longitudinal modes can be distinguished in the absorption spectrum calculated for an Au NPs array whereas such a feature is clearly observed for an Ag NPs array. The discrepancy between these two systems will be analyzed on the basis of a comparative study of their optical responses.

II. DISCRETE DIPOLE APPROXIMATION

The absorption spectra of metal NPs assembled in 2D hexagonal arrays are simulated using the DDA method. The detailed description of this method can be found elsewhere[26–29] as well as various arguments in favor of its applicability to simulate the optical properties of NPs.[29–31]

Briefly, the basic principle of the DDA was first applied by DeVoe in 1964 to calculate the optical properties of the molecular aggregates without considering the retardation effects.[26,27] In 1973, Purcell and Pennypacker considered the retardation effect to treat the interstellar dust grains.[28] Then, the theory has benefited from further improvements enabling to use the DDA method for calculating the absorption, extinction, and scattering cross sections of either individual or multiple objects with any size and shape.[29,32] Here, the free software DDSCAT 7.0 written by Draine and Flatau[33] is used to perform the DDA calculations.

A. Calculation of the absorption, extinction, and scattering cross sections

In the DDA approach, the system to be simulated, i.e., the target, is modeled as a periodic and finite (cubic) array of polarizable points whose spatial extension is fixed in such a way to mimic the shape of the object under investigation.[29] When such an array is placed under light exposure, each point ($j=1,2,\ldots,M$) acquires a dipole moment in response to the incident electric field, $\mathbf{E}_{inc,j}$. Let α_j stand for the polarizability of the jth dipole located at the position $\mathbf{r}_j$, therefore the polarization at this point is given by $\mathbf{P}_j=\alpha_j\mathbf{E}_j$ with the local electric field, $\mathbf{E}_j$ being expressed as

$$\mathbf{E}_j = \mathbf{E}_{inc,j} - \sum_{k\neq j} \mathbf{A}_{jk}\mathbf{P}_k, \tag{1}$$

where $-\mathbf{A}_{jk}\mathbf{P}_k$ corresponds to the electric field at the position $\mathbf{r}_j$ created by the dipole $\mathbf{P}_k$ at $\mathbf{r}_k$. Here, $\mathbf{A}_{jk}$ represents a (3 $\times$3) matrix whose elements are determined using the analytical expression

$$\mathbf{A}_{jk} = \frac{\exp(ikr_{jk})}{r_{jk}}\left[k^2(\hat{r}_{jk}\hat{r}_{jk}-\mathbf{1}_3) + \frac{ikr_{jk}-1}{r_{jk}^2}(3\hat{r}_{jk}\hat{r}_{jk}-\mathbf{1}_3)\right], \quad j\neq k, \tag{2}$$

where $k\equiv\omega/c$, $r_{jk}\equiv|\mathbf{r}_j-\mathbf{r}_k|$, $\hat{r}_{jk}\equiv(\mathbf{r}_j-\mathbf{r}_k)/r_{jk}$, and $\mathbf{1}_3$ is the (3$\times$3) identity matrix. Defining $\mathbf{A}_{jj}\equiv\alpha_j^{-1}$, Eq. (1) can also be written as the following system of linear complex equations:

$$\sum_{k=1}^{M} \mathbf{A}_{jk}\mathbf{P}_k = \mathbf{E}_{inc,j}. \tag{3}$$

After solving Eq. (3) for the unknown polarization $\mathbf{P}_j$, the extinction and absorption cross sections, C_{ext} and C_{abs}, are calculated by setting, respectively:

$$C_{ext} = \frac{4\pi k}{|\mathbf{E}_0|^2}\sum_{j=1}^{M} \mathrm{Im}(\mathbf{E}_{inc,j}^{*}\cdot\mathbf{P}_j), \tag{4}$$

$$C_{abs} = \frac{4\pi k}{|\mathbf{E}_0|^2}\sum_{j=1}^{M}\left\{\mathrm{Im}[\mathbf{P}_j\cdot(\alpha_j^{-1})^{*}\mathbf{P}_j^{*}] - \frac{2}{3}k^3|\mathbf{P}_j|^2\right\}. \tag{5}$$

The scattering cross section may also be determined by using $C_{sca}=C_{ext}-C_{abs}$.

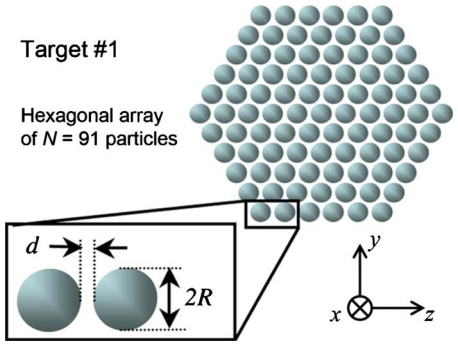

FIG. 1. (Color online) Schematic representation of the DDA target: two-dimensional hexagonal array composed of $N=91$ spheres (target 1) arranged in a hexagonal shape with a nearest-neighbor distance, d. The refractive index of the surrounding medium is set to that of dodecanethiol ($n_{ext}=1.46$).

B. Design of the target

The 2D assembly of metal NPs is represented by a planar hexagonal array of $N=91$ monosized spheres regularly spaced (target 1), as shown in Fig. 1. The interparticle spacing, d, denotes the border-to-border distance between two nearest-neighbor particles, while $2R$ is the particle diameter. In the following, the relative interparticle spacing is defined as the ratio of the interparticle spacing to the sphere diameter, that is, $d/(2R)$. Since the number of dipoles in the target conditions the calculation time, a compromise was required in order to ensure the accuracy of the calculations by choosing a fine meshing of the target without using too many dipoles. As seen from the modeling parameters listed in Table I, using a total number of around 2×10^5 dipoles in order to design target 1 enables us to reach an average number of 2000 dipoles per sphere while setting the interdipole spacing to values as small as 0.3 nm. Such a tiny value of the interdipole spacing ensures that it is much smaller than any characteristic structural feature of the system, thus making it possible to satisfactorily describe the NPs array. In addition, a previous study,[30] using simulation parameters similar to those given above, was found to enable the reasonable convergence of the DDA calculations. For this reason, the same meshing and limited number of particles in the array have been used for all the calculations presented in this work, whatever the interparticle spacing. In reference to the Au and Ag NPs coated by dodecanethiol that are experimentally synthesized in our group[34–36] using a chemical route, the refractive index of the medium surrounding the metal spheres is fixed at $n_{ext}=1.46$ for all the calculations.

TABLE I. Modeling parameters used for two different targets composed of M dipoles to form a hexagonal array of N spheres with an interparticle spacing given by $d/2R=0.2$. The number of peripheral spheres, N_P, and their relative proportion (%) are indicated, as well as the average number of dipoles per sphere, M/N.

Target	M	N	M/N	N_P (%)
1	234743	91	2580	30 (33)
2	1001839	469	2136	72 (15)

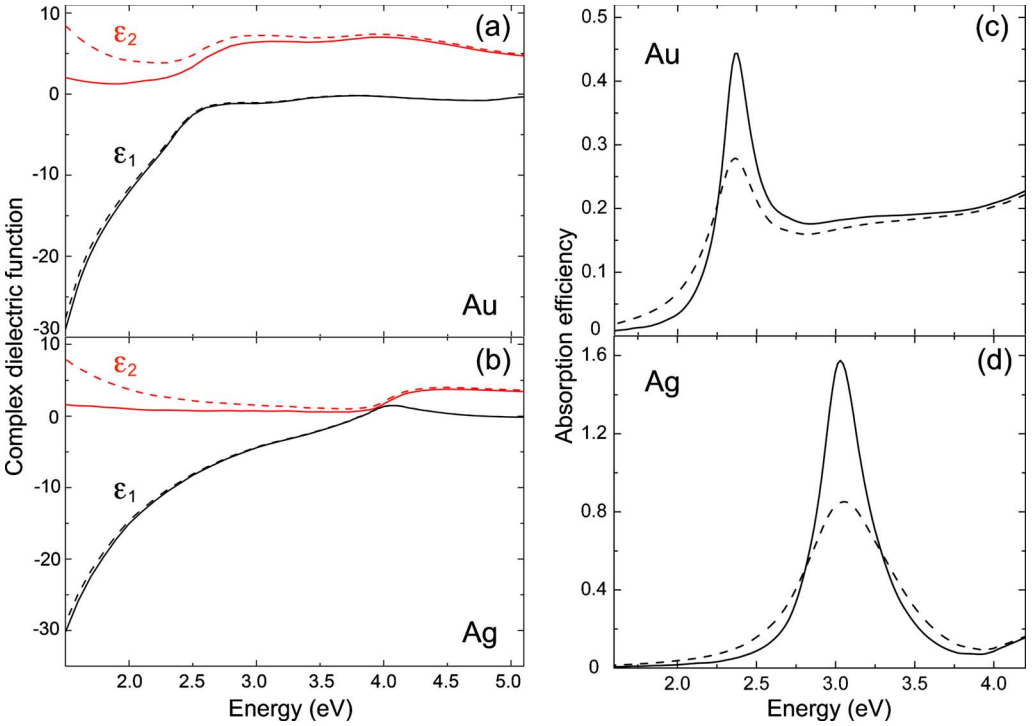

FIG. 2. (Color online) Real (ε_1) and imaginary (ε_2) components of the complex dielectric function of 5 nm (a) Au and (b) Ag NPs (dashed line) compared with those of bulk materials (solid line) from Ref. 40. Absorption spectra of individual (c) Au and (d) Ag spherical NPs, calculated by using either the size-corrected (dashed line) or the bulk dielectric function (solid line). The target used to simulate the particle is composed of 14 328 dipoles and the refractive index of the surrounding medium is fixed to $n_{ext}=1.46$.

C. Size-corrected dielectric function

The dielectric function $\varepsilon(\omega)$ of the target material needs also to be defined for the DDA calculation.[33] Generally, the dielectric function of real metals includes both the contributions of the bound and free electrons. Following the Drude model of a free-electron metal,[37,38] the dielectric function is given by

$$\varepsilon_{Drude}(\omega) = 1 - \frac{\omega_p^2}{\omega^2 + i\omega\gamma_0}, \tag{6}$$

where the plasma angular frequency $\omega_p = ne^2/\varepsilon_0 m_{eff}$ depends on both the electron density n, the effective mass m_{eff}, and a damping factor γ_0, which accounts for the scattering of electrons by phonons, electrons, lattice defects, or impurities. In nanometer-sized particles, an additional damping factor has to be introduced for the conduction electrons because of their scattering from the particle surface. As a consequence, the effective mean free path of the electrons, L_{eff}, is reduced as compared to the one in bulk metal. The resulting damping constant γ is therefore size dependent (via the introduction of L_{eff}) and can be expressed as

$$\gamma(L_{eff}) = \gamma_0 + A\upsilon_F/L_{eff}, \tag{7}$$

where A is a dimensionless factor whose value is determined by details of the scattering process and υ_F is the Fermi velocity. In order to account for such a surface dispersion effect, the dielectric function used for calculating the absorption spectra of metal nanoparticles is corrected by using the following relationship:[39]

$$\varepsilon(\omega, L_{eff}) = \varepsilon_{bulk}(\omega) - \varepsilon_{Drude}(\omega) + \left\{1 - \frac{\omega_p^2}{\omega^2 + i\omega(\gamma_0 + A\upsilon_F/L_{eff})}\right\}, \tag{8}$$

where $\varepsilon_{bulk}(\omega)$ is the bulk metal dielectric function. Here, the Au and Ag bulk dielectric functions are taken from Palik's handbook,[40] and the experimental values used for the Fermi velocity, the plasma energy, and the damping factor of each metal are from Ref. 41: (i) $\upsilon_F = 1.40 \times 10^6$ m/s, $\hbar\omega_p = 9.03$ eV, and $\gamma_0 = 0.024$ eV for Au; (ii) $\upsilon_F = 1.39 \times 10^6$ m/s, $\hbar\omega_p = 8.98$ eV, and $\gamma_0 = 0.018$ eV for Ag. Following a geometrical probability approach,[38] the effective electron mean free path of the conduction electrons inside a spherical particle of radius R is simply stated as $L_{eff} = 4R/3$. As usually assumed, the constant A has been set to unity when using Eq. (8) for the calculation of the size-corrected dielectric functions involved in this work.

To illustrate the size dependence of the dielectric function, the real (ε_1) and imaginary (ε_2) parts of the size-corrected complex dielectric functions calculated for Au and Ag 5 nm spherical NPs are compared in Figs. 2(a) and 2(b) with those of bulk metals. While the real part of the dielectric function exhibits very low size dependence, the imaginary part is sensitively affected in the range below 4 eV by the size correction given by Eq. (8). Due to the surface dispersion effect just mentioned above, the SPRs of both Au and Ag spherical NPs, which emerge in the visible range, are likely to depend on their size. The optical absorption spectra calculated by using either the size corrected or the bulk dielectric function

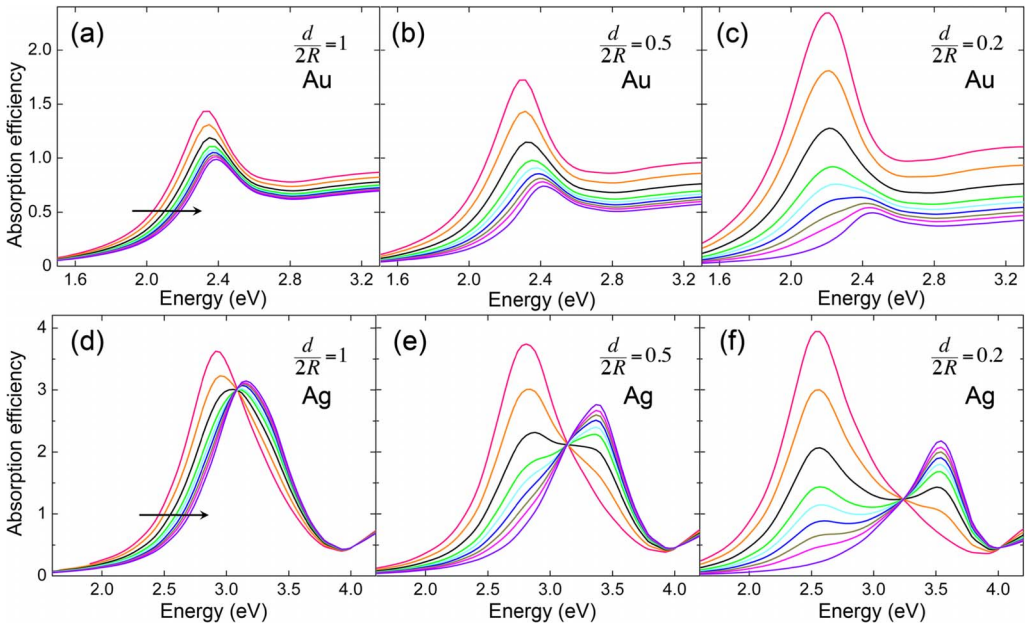

FIG. 3. (Color online) Dependence on the incident angle of the absorption spectra of (a)–(c) Au and (d)–(f) Ag spheres of 5 nm diameter assembled in 2D arrays for three different relative interparticle spacings: (a) and (d) $d/(2R)=1$, (b) and (e) $d/(2R)=0.5$, and (c) and (f) $d/(2R)=0.2$. For each case, the following incidence angles are considered: 0° (pink), 30° (orange), 45° (black), 55° (green), 60° (cyan), 65° (blue), 70° (olive), 75° (magenta), and 90° (violet). The arrows are oriented in the sense of increasing incidence angle.

of individual Au and Ag NPs are compared in Figs. 2(c) and 2(d). Here, the particles are considered to be surrounded by a medium with the same refractive index as the one of dodecanethiol ($n_{ext}=1.46$). For both metals, the position of the SPR remains almost unchanged whatever the dielectric function used. The unique SPR band of individual Au NPs emerging in the spectra of Fig. 2(c) is peaked at 2.37 eV, and that of Ag NPs appears around 3.0 eV in Fig. 2(d). In contrast with the invariance of the SPR position, both its amplitude and width exhibit dramatic change when taking into account the size dependence of the dielectric function in the DDA calculation. As a matter of fact, a slight broadening of the SPR is observed as well as a strong decrease in its amplitude. Such a damping of the SPR of metal particles observed for decreasing size qualitatively agrees with experimental measurements performed on noble-metal NPs with a few nanometers in diameter[42] and makes sense for using the size-corrected dielectric function in the simulation presented in this work.

III. RESULTS AND DISCUSSION

The absorption spectra calculated for a 2D self-organization of NPs composed of $N=91$ spheres uniformly sized and assembled in a regular planar hexagonal array are now considered. The incident light propagates along the x axis with the electric field vector being oriented in the y-axis direction (see Fig. 1). When the incident angle, θ, is fixed at 0°, i.e., at normal incidence, the hexagonal array stands parallel to the (yz) plane with the electric field being also parallel to the latter, which corresponds to the so-called *in-plane* configuration. In order to simulate a change in the incident angle, the hexagonal array is simply rotated around the z axis. In this way, the *out-of-plane* configuration is therefore obtained by considering the light propagation at grazing incidence, that is, by setting the angle of incidence at 90°. In such a configuration, the incident light propagates parallel to the hexagonal array. The interparticle spacing, d, is defined as the border-to-border distance between two nearest-neighbor particles, and $2R$ is the particle diameter.

Figures 3(a)–3(c) show the absorption spectra of 5 nm Au NPs organized in a hexagonal array. Only one single SPR band is observed for any the incidence angle and interparticle spacing. At normal incidence ($\theta=0°$), the electric field of the light is parallel to the plane of the NPs array (in-plane configuration). Hence, the absorption band is ascribed to the longitudinal plasmon resonance in the NPs array. On increasing the incidence angle, the SPR band slightly shifts toward higher energies. Note that the blue shift of the SPR band is mainly appreciable when looking at large incidence angles ($65° \leq \theta \leq 90°$). Furthermore, the profile of the SPR band is observed to depend on the incidence angle, especially for the more compact array characterized by an interparticle spacing of $d/(2R)=0.2$, as illustrated in Fig. 3(c). This change in the SPR band profile can be attributed to the increasing contribution of the absorption related to the transverse plasmon resonance when progressively rotating the planar array from an in-plane to out-of-plane configuration. Concerning the dependence of the absorption spectrum on the interparticle spacing, it is surprising to observe no splitting of the SPR band when decreasing the interparticle spacing in the Au NPs array, in contrast with previous studies of the optical response of Ag NPs organized in 2D planar arrays.[30,43,44] Indeed, it is common knowledge that the strength of the dipolar interaction between the NPs in the array is primarily governed by the interparticle spacing so that the greater the in-

terparticle spacing, the weaker the dipolar interactions between the neighboring NPs. Conversely, decreasing the interparticle spacing leads to strengthening the interactions between NPs and, consequently, favors the emergence of collective optical properties. From this fact, it is expected that both the energies of the two plasmon resonances and their respective amplitudes would exhibit dependence on the interparticle spacing.

In order to illustrate and ascertain the arguments mentioned above concerning the dependence of the SPR spectrum of Au NPs array on both the incidence angle and interparticle spacing, let us compare the results shown before with those obtained for Ag NPs organized in similar arrays. The corresponding absorption spectra are shown in Figs. 3(d)–3(f). Comparing first Figs. 3(a) and 3(d), it appears that the SPR spectra of Au and Ag NPs arrays with an interparticle spacing of $d/(2R)=1$ exhibit the same dependence on the incidence angle since, for both cases, one observes one single SPR band which is blueshifted for increasing incidence. However, a further comparison of these two systems for shorter interparticle spacings reveals several discrepancies between their optical responses. As shown in Fig. 3(f) for $d/(2R)=0.2$ and to a lesser extent in Fig. 3(e) for $d/(2R)=0.5$, two bands emerge in the SPR spectra of Ag NPs array for incidences ranging from 30° to 75°. Indeed, in addition to the lower energy band related to the longitudinal plasmon resonance, which is centered around 2.5 eV, a second band distinctly emerges at higher energy (≈3.5 eV) and progressively grows on increasing the incidence angle. This band is attributed to the transverse plasmon resonance of the Ag NPs array. Both the longitudinal and transverse plasmon resonances are therefore well distinguished in the spectra of Ag NPs array with an interparticle spacing not exceeding one particle radius, in contrast with similar arrays of Au NPs whose spectra are displayed in Figs. 3(b) and 3(c). As a matter of fact, the energy difference, ΔE, between the transverse ($E_\perp$) and longitudinal ($E_\parallel$) plasmon energies of the Ag NPs array is large enough to allow clear observation of an isosbestic point in Figs. 3(d)–3(f) whereas no such feature is observed for the Au NPs array for any interparticle spacing, due to the weaker splitting between the two plasmon modes in the latter system. At this point, it should be noted that, unlike the case of Ag, both the transverse and longitudinal plasmon resonances of the Au NPs array emerge above the threshold of the interband electronic transitions (1.84 eV). Hence, the two plasmon resonance bands are superimposed on the tail of the interband transitions absorption inducing the subsequent broadening of the two plasmon bands and making therefore their splitting even more difficult to observe with Au as compared to Ag NPs arrays.

Although the bands related to the longitudinal and transverse plasmon resonances are not discernible for the Au NPs array, their respective amplitudes are expected to vary with the interparticle spacing, as was previously shown for their energies. This variation in the two plasmon resonances amplitudes could be estimated from the evolution of the spectra profile depicted in Figs. 3(a)–3(c). Nevertheless, in order to better illustrate the dependence of both the amplitudes and splitting of the two plasmon resonances on the interparticle distance, Fig. 4 shows how the "strict" longitudinal and

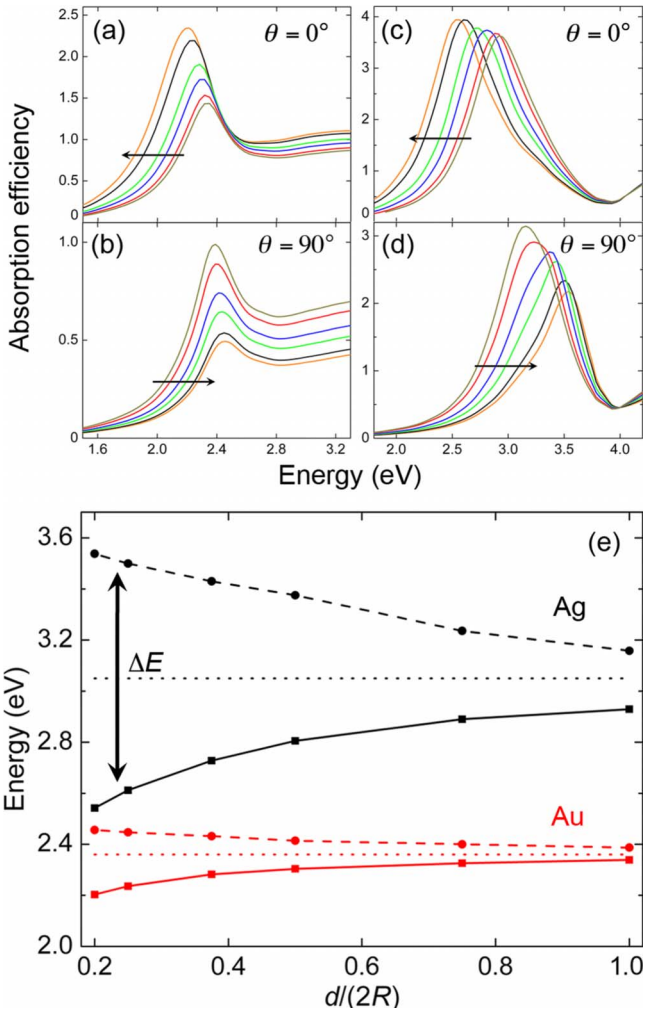

FIG. 4. (Color online) Calculated absorption spectra of 5 nm (a) and (b) Au and (c) and (d) Ag NPs ordered in 2D arrays of 91 NPs for (a) and (c) normal and (b) and (d) parallel incidences for various relative interparticle spacings $d/(2R)$: 0.2 (orange), 0.25 (black), 0.375 (green), 0.5 (blue), 0.75 (red), and 1 (olive). The arrows are oriented in the sense of decreasing $d/(2R)$. (e) Plot of both the longitudinal (solid lines) and transverse (dashed lines) SPR versus $d/(2R)$ for Au (red) and Ag (black) NPs arrays. The dotted horizontal lines indicate the SPR energy of an individual 5 nm spherical NP.

transverse plasmon resonances evolve for both Au and Ag NPs arrays. Actually, plotting the absorption spectra calculated for different $d/(2R)$ values and for an incidence angle of either 0° or 90° enables independently following the longitudinal and transverse plasmon resonances dependence on the compactness of the array. As shown in Figs. 4(a) and 4(c), at normal incidence, the longitudinal resonance is shifted toward lower energies and is also amplified for decreasing interparticle spacing. Conversely, at parallel incidence, Figs. 4(b) and 4(d) clearly exhibit a blue shift of the transverse plasmon resonance accompanied by a significant decrease in its amplitude when the interparticle spacing decreases. On comparing the evolution of the spectra of the Au NPs array in Figs. 4(a) and 4(b) to those of the Ag NPs array in Figs. 4(c) and 4(d), it is seen that the variation in the

TABLE II. Energies of the longitudinal ($E_{\parallel}$) and transverse ($E_{\perp}$) plasmon resonances and energy differences ($\Delta E = E_{\perp} - E_{\parallel}$) determined graphically from the absorption spectra of Au and Ag NPs arrays shown in Fig. 4.

		$d/(2R)$					
		0.2	0.25	0.375	0.5	0.75	1
Ag	$E_{\perp}$	3.54	3.50	3.43	3.38	3.24	3.16
	$E_{\parallel}$	2.54	2.61	2.73	2.81	2.89	2.93
	$\Delta E^{(Ag)}$	1.00	0.89	0.70	0.57	0.35	0.23
Au	$E_{\perp}$	2.46	2.45	2.43	2.41	2.40	2.39
	$E_{\parallel}$	2.20	2.24	2.28	2.30	2.33	2.34
	$\Delta E^{(Au)}$	0.26	0.21	0.15	0.11	0.07	0.05

interparticle spacing of the two resonances energy is more sensitive for Ag NPs arrays. Conversely, the amplitude is found to vary much more sensitively for the Au compared to the Ag NPs array.

Plotting the data listed in Table II enables us to follow the respective evolution of the longitudinal and transverse plasmon resonance energies with the relative interparticle spacing, as presented in Fig. 4(e). The curves plotted in this graph clearly illustrate the variation in the energy difference ΔE characterizing the splitting between the two resonances for both systems. From the comparison given in Fig. 4(e), the splitting is well demonstrated to significantly depend on the compactness of the 2D NPs array for both Ag and Au metals. Furthermore, these data also point out the larger splitting measured for an Ag compared to an Au NPs array, confirming the different optical behaviors of the two metals.

To improve the accuracy of the calculations presented above in view to support their validity for simulating the optical absorption spectra of metal NPs close packed in planar arrays, additional calculations have been carried out by using a more extended target, namely, target 2, which consists in an hexagonal array of $N=469$ NPs, as shown in Fig. 5(a). The modeling parameters characterizing this second target are compared to those of target 1 in Table I. Note that a total number of around 10^6 dipoles was used to design target 2, making therefore the average number of dipoles per sphere comparable to that of target 1 ($M/N > 2000$ dipoles/sphere). This precaution aims to avoid any spurious effect that might originate from a rough meshing of the target and allows directly comparing the spectra calculated using these two targets in order to examine their dependence on the modeling parameters. Figures 5(b) and 5(c) present a comparison of the spectra calculated using these two targets for Au and Ag, respectively. From this comparison, one remarks in both cases a slight evolution of the SPR profile when increasing the number of particles in the target from $N=91$ up to 469 NPs. In particular, the width of the SPR bands appears a bit broader for target 2. In contrast, it is also important to note, especially from the comparison shown in Fig. 5(c), that both the energies and relative intensities of the transverse and longitudinal plasmon resonances are quasi unchanged. Consequently, these last results reveal that the splitting of the SPR does not depend on the relative proportion of peripheral NPs in the target. Thus, under the requirement that a reasonably high number of particles should be used to model the target, the finite extension of this latter does not affect the capability of the DDA method for

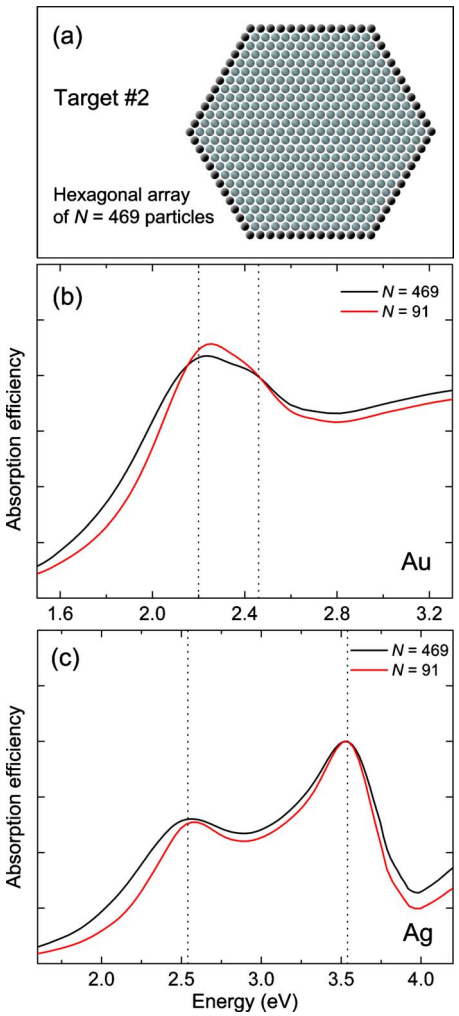

FIG. 5. (Color online) (a) Schematic view of target 2 consisting of a hexagonal planar array of $N=469$ NPs of which 72 (black ones) are located on the periphery. (b) Comparison of the absorption spectra calculated for target 1 (red curve) and target 2 (black curve) consisting in $N=91$ and 469 Au NPs, respectively. (c) Same as previous for Ag NPs arrays. The dotted lines indicate the $E_{\perp}$ and $E_{\parallel}$ SPR energies determined from the graphs plotted in Fig. 4.

simulating the optical properties of metal NPs planar arrays.

IV. CONCLUSION

In summary, we have performed a comparative study, by the DDA method, of the collective optical properties of 5 nm Au and Ag NPs self-organized in hexagonal planar arrays. The absorption spectra calculated for Au NPs arrays exhibit one single SPR band for any interparticle spacing, whereas those of Ag NPs arrays clearly reveal two bands corresponding to the longitudinal and transverse plasmon resonances for interparticle spacings not exceeding one particle radius. We show that strengthening the dipolar NPs interactions by decreasing the interparticle spacing results in a weaker splitting between the two resonance modes for Au NPs arrays as compared to Ag ones, while the resonance amplitude is conversely found to be much more sensitive to the interparticle spacing for the former. Consequently, it is expected that real close-packed planar arrays of Au NPs with size limited to a few nanometers will exhibit no splitting of the SPR band in their absorption spectra, making it therefore difficult to detect any effect related to their optical anisotropy through classical absorption measurements. Beyond some limitations for producing and properly characterizing real close-packed arrays of Au and Ag nanoparticles deposited on a substrate, a further experimental investigation is planned to compare their optical responses with that predicted via the DDA simulations.

ACKNOWLEDGMENTS

P.Y. thanks China Scholarship Council for the financial support. The authors thank N. Pinna (University of Aveiro, Portugal) for helpful discussions and the usage of computing resources. The authors express their gratitude to B. T. Draine (Princeton University) and P. J. Flatau (University of California) for the free DDA software (DDSCAT 7). This work was partly supported by ANR in the frame of the PION research program (Project No. BLAN06-1_147266).

*Corresponding author; marie-paule.pileni@upmc.fr

[1] M. Faraday, Philos. Trans. R. Soc. London, Ser. B **147**, 145 (1857).
[2] E. Hao, G. C. Schatz, and J. T. Hupp, J. Fluoresc. **14**, 331 (2004).
[3] L. Bonacina, A. Callegari, C. Bonati, F. van Mourik, and M. Chergui, Nano Lett. **6**, 7 (2006).
[4] V. Torres, M. Popa, D. Crespo, and J. M. C. Moreno, Microelectron. Eng. **84**, 1665 (2007).
[5] S. A. Maier, M. L. Brongersma, P. G. Kik, S. Meltzer, A. A. G. Requicha, and H. A. Atwater, Adv. Mater. **13**, 1501 (2001).
[6] P. K. Jain, X. Huang, I. H. El-Sayed, and M. A. El-Sayed, Acc. Chem. Res. **41**, 1578 (2008).
[7] P. K. Jain and M. A. El-Sayed, Nano Lett. **8**, 4347 (2008).
[8] A. J. Haes and R. P. Van Duyne, J. Am. Chem. Soc. **124**, 10596 (2002).
[9] X. H. Huang, I. H. El-Sayed, W. Qian, and M. A. El-Sayed, J. Am. Chem. Soc. **128**, 2115 (2006).
[10] J. Chen, F. Saeki, B. J. Wiley, H. Cang, M. J. Cobb, Z.-Y. Li, L. Au, H. Zhang, M. B. Kimmey, X. Li, and Y. Xia, Nano Lett. **5**, 473 (2005).
[11] J. J. Mock, M. Barbic, D. R. Smith, D. A. Schultz, and S. Schultz, J. Chem. Phys. **116**, 6755 (2002).
[12] K. L. Kelly, E. Coronado, L. L. Zhao, and G. C. Schatz, J. Phys. Chem. B **107**, 668 (2003).
[13] Y. S. Lee, *Self-Assembly and Nanotechnology: A Force Balance Approach* (Wiley, Hoboken, NJ, 2008).
[14] *Nanocrystals Forming Mesoscopic Structures*, edited by M.-P. Pileni (Wiley-VCH, Weinheim, Germany, 2005).
[15] C. P. Collier, R. J. Saykally, J. J. Shiang, S. E. Henrichs, and J. R. Heath, Science **277**, 1978 (1997).
[16] L. L. Zhao, K. L. Kelly, and G. C. Schatz, J. Phys. Chem. B **107**, 7343 (2003).
[17] A. N. Shipway, E. Katz, and I. Willner, ChemPhysChem **1**, 18 (2000).
[18] A. N. Shipway and I. Willner, Chem. Commun. (Cambridge) **2001**, 2035.
[19] J. J. Storhoff, A. A. Lazarides, R. C. Mucic, C. A. Mirkin, R. L. Letsinger, and G. C. Schatz, J. Am. Chem. Soc. **122**, 4640 (2000).
[20] T. Teranishi, C. R. Chim. **6**, 979 (2003).
[21] T. Sen and A. Patra, J. Phys. Chem. C **113**, 13125 (2009).
[22] L. Polavarapu and Q. H. Xu, Langmuir **24**, 10608 (2008).
[23] S. Lin, M. Li, E. Dujardin, C. Girard, and S. Mann, Adv. Mater. **17**, 2553 (2005).
[24] C. Y. Jiang, S. Markutsya, and V. V. Tsukruk, Langmuir **20**, 882 (2004).
[25] J. Schmitt, G. Decher, W. J. Dressick, S. L. Brandow, R. E. Geer, R. Shashidhar, and J. M. Calvert, Adv. Mater. **9**, 61 (1997).
[26] H. DeVoe, J. Chem. Phys. **41**, 393 (1964).
[27] H. DeVoe, J. Chem. Phys. **43**, 3199 (1965).
[28] E. M. Purcell and C. R. Pennypacker, Astrophys. J. **186**, 705 (1973).
[29] B. T. Draine and P. J. Flatau, J. Opt. Soc. Am. A Opt. Image Sci. Vis. **11**, 1491 (1994).
[30] H. Portalès, N. Pinna, and M.-P. Pileni, J. Phys. Chem. A **113**, 4094 (2009).
[31] P. Yang, H. Portalès, and M.-P. Pileni, J. Phys. Chem. C **113**, 11597 (2009).
[32] J. J. Goodman, B. T. Draine, and P. J. Flatau, Opt. Lett. **16**, 1198 (1991).
[33] B. T. Draine and P. J. Flatau, arXiv:0809.0337v4 (unpublished).
[34] H. Portales, N. Goubet, L. Saviot, S. Adichtchev, D. B. Murray, A. Mermet, E. Duval, and M.-P. Pileni, Proc. Natl. Acad. Sci. U.S.A. **105**, 14784 (2008).
[35] N. Goubet, Y. Ding, M. Brust, Z. L. Wang, and M.-P. Pileni, ACS Nano **3**, 3622 (2009).
[36] A. Taleb, C. Petit, and M. P. Pileni, Chem. Mater. **9**, 950 (1997).
[37] C. F. Bohren and D. R. Huffman, *Absorption and Scattering of*

Light by Small Particles (Wiley-VCH, Berlin, 1998).
[38] E. A. Coronado and G. C. Schatz, J. Chem. Phys. **119**, 3926 (2003).
[39] H. Hovel, S. Fritz, A. Hilger, U. Kreibig, and M. Vollmer, Phys. Rev. B **48**, 18178 (1993).
[40] E. D. Palik, *Handbook of Optical Constants of Solids* (Academic, New York, 1985).
[41] N. W. Ashcroft and N. D. Mermin, *Solid State Physics*, International ed. (Holt-Saunders, Philadelphia, 1976).
[42] E. Cottancin, G. Celep, J. Lerme, M. Pellarin, J. R. Huntzinger, J. L. Vialle, and M. Broyer, Theor. Chem. Acc. **116**, 514 (2006).
[43] H. Wormeester, A.-I. Henry, E. S. Kooij, B. Poelsema, and M.-P. Pileni, J. Chem. Phys. **124**, 204713 (2006).
[44] N. Pinna, M. Maillard, A. Courty, V. Russier, and M. P. Pileni, Phys. Rev. B **66**, 045415 (2002).